Plant Physiology and Biochemistry 143 (2019) 50–60

Contents lists available at ScienceDirect

Plant Physiology and Biochemistry

journal homepage: www.elsevier.com/locate/plaphy

Research article

Deciphering the biological processes underlying tomato biomass production and composition

Daniela D'Esposito[a], Elisa Cappetta[a], Giuseppe Andolfo[a], Francesca Ferriello[a], Camilla Borgonuovo[a], Gianluca Caruso[a], Antonino De Natale[b], Luigi Frusciante[a], Maria Raffaella Ercolano[a,*]

[a] Department of Agricultural Sciences, University of Naples 'Federico II', Via Università 100, 80055, Portici, Naples, Italy
[b] Department of Biology, University of Naples 'Federico II', Via Cinthia, Monte Sant'Angelo, Building 7, 80126, Naples, Italy

ARTICLE INFO

Keywords:
Biomass
Cell wall
Introgression lines
Plant growth
Saccharification
S. lycopersicum

ABSTRACT

The huge amounts of biomass residues, remaining in the field after tomato fruits harvesting, can be utilized to produce bioenergy. A multiple level approach aimed to characterize two *Solanum pennellii* introgression lines (ILs), with contrasting phenotypes for plant architecture and biomass was carried out. The study of gene expression dynamics, microscopy cell traits and qualitative and quantitative cell wall chemical compounds variation enabled the discovery of key genes and cell processes involved biomass accumulation and composition. Enhanced biomass production observed in IL2-6 line is due to a more effective coordination of chloroplasts and mitochondria energy fluxes. Microscopy analysis revealed a higher number of cells and chloroplasts in leaf epidermis in the high biomass line whilst chemical measurements on the two lines pointed out striking differences in the cell wall composition and organization. Taken together, our findings shed light on the mechanisms underlying the tomato biomass production and processability.

1. Introduction

The biomass derived from waste and agricultural residues represents an important source of renewable energy since large scale energy crops, used for electricity or heat production, showed to highly impact the environment and agricultural production (Koçar and Civaş, 2013; Gomez et al., 2017). Plant biomass is generated through the process of photosynthesis in which the readily available carbon dioxide (CO_2) from the air and soil water are combined to produce carbohydrates, which represent the biomass "building blocks" (Mckendry, 2002). Photosynthesis takes place inside the chloroplasts and it is divided in two steps, the first phase comprises light uptake and electron transport around photosystems, the second phase is related to CO_2 assimilation in Calvin-Benson Cycle. The solar energy that drives photosynthesis is stored in the chemical bonds of the carbohydrates and other molecules contained in the biomass (Mckendry, 2002; Zhou et al., 2011; Baskar et al., 2012). Sucrose transport and hydrolysis play key regulatory roles in carbon (C) allocation and sugar signal generation (Ruan, 2014), promoting the cell proliferation and cell wall synthesis and leading to increased plant growth and biomass accumulation (Tognetti et al., 2013; Maloney et al., 2015). Although sucrose is the major photosynthetic product, several effects on growth and metabolism can be attributed to starch degradation (Fernandez et al., 2017).

Plant development and growth promotion are mediated by hormones such as auxin (IAA), gibberellins (GAs), and brassinosteroids (BRs) through a sophisticated cross regulation (Ross and Quittenden, 2016). Recent studies highlight the role of different transcription factors (TFs) families like Auxin Response Factors (ARFs), SMALL AUXIN UP RNA (SAUR), Growth Regulating Factors (GRFs) and MAD-box in modulating developmental processes such leaf morphogenesis, switch from vegetative to reproductive phase and coordination of growth activities (Kim et al., 2003; Pajoro et al., 2014; Omidbakhshfard et al., 2015). Plant can undergo reiterative growth and continuous organogenesis thanks to the axillary meristems (AMs) that play a central role in meristem initiation and exhibition of plant architecture diversity in which members of HD-ZIP-III and MYB TF families are important regulators (Yang and Jiao, 2016). The growth is also promoted by high cell division rate and short duration of cell cycle phases (Sablowski and

* Corresponding author.
E-mail addresses: danieladesposito@hotmail.it (D. D'Esposito), elisa.cappetta@unina.it (E. Cappetta), giuseppeandolfo@hotmail.com (G. Andolfo), francesca.ferriello@unina.it (F. Ferriello), camilla.borgonuovo@gmail.com (C. Borgonuovo), gcaruso@unina.it (G. Caruso), antonino.denatale@gmail.com (A. De Natale), fruscian@unina.it (L. Frusciante), ercolano@unina.it (M.R. Ercolano).

https://doi.org/10.1016/j.plaphy.2019.08.010
Received 23 May 2019; Received in revised form 19 July 2019; Accepted 13 August 2019
Available online 13 August 2019

Carnier Dornelas, 2014). The cell cycle progression is tightly regulated by molecular components with a pivotal role of the TF E2F at the G1/S transition, modulating the expression of genes involved in DNA replication and chromatin dynamics (De Veylder et al., 2007) and the anaphase-promoting complex (APC) triggering the transition from metaphase to anaphase and the exit from mitosis (Inzé, 2003; Lima et al., 2010; Wade Harper et al., 2002; Eloy et al., 2015).

The majority of energy stored in plant biomass, through the regulation of photosynthesis, C metabolism and organ allocation, is contained within the dense polymers of the cell wall, consisting primarily of carbohydrate polymers such as cellulose and hemicellulose and the polyphenol-based lignin (Mckendry, 2002; Slavov et al., 2013) also called lignocellulosic biomass. Many studies have shown that lignocellulosic biomass holds enormous potential for sustainable production of biofuels (Somerville et al., 2010; Sorek et al., 2014; Isikgor and Becer, 2015). Biomass of agricultural residues can be conserved, managed, and utilized to produce bioenergy (Vanholme et al., 2013; Aro, 2016; Peña-Castro et al., 2017). Among the major vegetable crops worldwide there are few evidences for using tomato residues for biofuel production (Ercolano et al., 2015). The phenotypic and chemical assessment of a set of *S. pennellii* introgression lines (ILs), derived from the cross with *S. lycopersicum* cv. M82 (Eshed and Zamir, 1995), provided useful information about tomato biomass production and its potential use in fuel conversion (Caruso et al., 2016).

In this study, we further investigated two *S. pennellii* ILs (IL2-6 and IL3-2) that greatly differed in the morphology (plant growth/architecture), physiology and also in the saccharification rate, with IL2-6 not only having the higher production of residual biomass but also the more efficient hydrolysis of biomass to fermentable sugars. They can be considered nearly isogenic lines except for the contribute of *S. pennellii* introgressed genomic region (IGR). A multilevel characterization, including transcriptomic, chemical and morphological analysis allowed us to highlight the gene regulatory network underlying pathways involved in traits related to biomass production. We focused our analyses on the photosynthesis and energy fluxes activated to sustain plant growth. The complex cycles triggered from chloroplast supply were investigated to understand how the leaf cell morphology, the plastid organization and the chemical assembly of cell wall components can affect tomato biomass production and hydrolysis.

2. Materials and methods

2.1. Plant material

The M82 variety, the tomato line IL2-6, that has the same genetic background of M82 except for a region of 3.7 Mb of *S.pennelli* chromosome 2 (from genome coordinates SL2.50ch02:51151577 to SL2.50ch02:54885529), and the line IL3-2, that differs from M82 for a region of 58.9 Mb of *S.pennelli* chromosome 3 (from SL2.50ch03:1440138 to SL2.50ch03:60439411), were used for our experiments. The lines were kindly provided by Dr. Dani Zamir (Hebrew University of Jerusalem) Plants of three genotypes were grown in open field (40.50° N, 14.15° E, 17 m a.s.l.) in 2011 and 2012 on a sandy-loam soil field under Mediterranean climate (Peel et al., 2007). A randomized complete block design with three replicates of 7–9 plants each was used. Plants were transplanted on 20 and 18 April in 2011 and 2012 respectively and arranged in single rows spaced by 0.90 m from each other with 30 cm spacing between plants along the rows, with an areal density of 3.2 m^2. Each year the plants were supplied with 106 kg ha^{-1} N, 32 kg ha^{-1} P_2O_5 and 160 kg ha^{-1} K_2O. Drip irrigation was activated when the soil available water capacity (AWC) decreased to 70%. Fruits were harvested at full ripening. Agronomic collected data (fruit yield, mean fruit weight and number of fruits per plant, residual biomass, including discarded fruits per plant) are reported in Caruso et al. (2016). Samples of residual biomass belonging to the same genotype were collected and pooled per replicate to conduct further analysis. A part was used to conduct phenotypic evaluation, the remaining was divided into replica aliquots and dried in an oven at 70 °C under vacuum milled and stored in air-tight bags at −20 °C for chemical analysis or frozen under liquid nitrogen and then stored at −80 °C for RNA sequencing.

2.2. Total RNA extraction and sequencing

Total RNA was extracted from leaf tissue of IL2-6, IL3-2 and M82 varieties (three biological replicates per genotype) using the Spectrum plant total RNA Kit (Sigma-Aldrich, St. Louis, MO, USA) and treated with DNase I (Sigma-Aldrich) to remove contaminant DNA. cDNA synthesis was performed with oligo (dT) and SuperScript III Reverse Transcriptase (Invitrogen, Carlsbad, CA, USA). All RNA samples were quantified with NanoDrop ND-1000 spectrophotometer (NanoDrop Technologies, Wilmington, DE, USA) and RNA quality (integrity) was assessed with an Agilent 2100 Bioanalyzer (Agilent Technologies, Santa Clara, CA, USA). For the samples IL3-2 and M82 the RNA sequencing included unstranded library preparation with TruSeq Standard mRNA kit (Illumina, San Diego, CA, USA) followed by 50 base pair (bp) single-end reads sequencing at Sequentia Biotech SL, Barcelona, Spain. A single end tag sequencing strategy was chosen, in which short tags were extracted from the ends of long DNA fragments for ultra-high-throughput sequencing. For the sample IL2-6 the RNA was used for indexed libraries preparation with TruSeq Stranded mRNA Kit (Illumina), and each library was subjected to a paired-end sequencing (2 x 100 bp) at Genomix4life, Baronissi (SA) - Italy (www.genomix4life.com). All libraries were sequenced on the Illumina HiSeq1500 platform.

2.3. Mapping and differential expression analysis

Raw sequencing reads were subjected to a quality check in order to obtain high quality reads. Sequence adapters were trimmed and reads with a quality score below 25 and a length below 35 bp and with ambiguous bases 'N' were removed using the preprocessing tool Trimmomatic (Bolger et al., 2014a). Two M82 replicas failed the quality control and were removed from the data analysis. The high quality reads (clean reads) were aligned to *S. lycopersicum* cv Heinz (version SL2.50) and *S. pennellii* LA0716 (Bolger et al., 2014b) reference genome assemblies using the splice read mapper TopHat2 (Kim et al., 2013) software (v2.0.12).

The resulting alignment files were used as input for HT-seq with default setting (Anders et al., 2015) together with annotation (ITAG2.4 and SPENN_v2.0) files to calculate gene expression values (raw read counts). The strand-specific assay of different RNA-Seq libraries was specified (option –s).

The R package CQN (conditional quantile normalization) [36] was used to normalize HT-seq read counts. The edgeR package (http://www.r-project.org/) (Robinson et al., 2009) was used to identify the differentially expressed genes (DEGs) between the two lines. Genes with a false discovery rate (FDR) < 0.05, using Benjamini and Hochberg (1995) method, were considered significant DEGs. Only the reliable mapped reads, resulting from the alignment with TopHat2 (as described above), were considered for Single Nucleotide Polymorphisms (SNPs). The SNP and Indel positions within the aligned reads compared to the reference genome were identified using the pileup function in SAMtools v1.9 (Li et al., 2009). The SNPs were further filtered using a minimum SNP quality score (QUAL), mapping quality (MQ) and genotype quality (GQ) of 30, an allele frequency (AF) higher than 0.75 and a minimum and maximum read depths (coverage) setted to 5 and 100, respectively (Supplementary Fig. S1).

2.4. Pairwise orthology analysis

Orthology analysis was conducted on proteomes of tomato (*S. lycopersicum* cv Heinz ITAG2.5) and *S.pennelli* (SPENN_v2.0) using

Inparanoid software with default parameters (Remm et al., 2001; Alexeyenko et al., 2006). We used a confidence score threshold equal to one to directly estimate orthology relationships between the identified ortholog genomic regions.

2.5. Functional annotation of DEGs

Gene Ontology (GO) enrichment analysis of DEGs was performed using the R package TopGO (Alexa and Rahnenfuhrer, 2018). GO background for *Solanum lycopersicum* genes (SL2.50) was downloaded from Ensemble Plant Genes release 41 (http://plants.ensembl.org, Ensembl Genomes release 41 - September 2018), accounting for the functional annotation of genes located on chromosomes 1–12. The missing GO annotation for genes of "chromosome 0" was integrated with interproscan results (November 2018) from PLAZA 4.0 dicots (Van Bel et al., 2018), available at https://bioinformatics.psb.ugent.be/plaza. DEGs mapping to metabolic pathway was performed by combining informations from MapMan 3.0.0 tool (Thimm et al., 2004) and Plant MetGenMAP pathways (http://bioinfo.bti.cornell.edu/cgi-bin/MetGenMAP/home.cgi) (Joung et al., 2009).

2.6. Miscroscopy analysis

Fully expanded leaves from three replicas of the two ILs (IL2-6 and IL3-2) were used for cell morphological measurements. From each plant three fully-grown leaves were taken from the middle part of the stem samples of mature leaves were fixed in 70% ethanol (for 24 h at room temperature). Small pieces, approximately 1 cm^2, of each tomato line leave were cut from the central region of the lamina close to the middle of middle rib. Leaf samples were incorporated into elder marrow. Sections 10 μm thick were cut using a hand microtome (Eleitz Wetzlar, Germany), mounted on glass slides before observing with a light microscope (Nikon Eclipse E800). For each IL, 10 sections of leaf tissue were examined using 10x, 40x and 100× objectives. Photomicrographs of the sections were taken using a Nikon DXM 1200 digital camera (Tokyo, Japan) with micrometric scales that were photographed and magnified under the same optical conditions used for the sections. The photographic documentation was used for computer image analysis, with the basic plugins of Fiji software (http://www.fiji.sc) [46], to evaluate the size of palisade and spongy mesophyll cells. Other measurements were made on the individual chloroplasts and on the total content inside the cells. The difference between the two lines regarding chloroplasts and epidermal cells (palisade and spongy) characteristics was tested by the Student's test (P-value < 0.05).

2.7. Chemical analysis of lignocellulosic biomass

Cell wall composition of IL line is reported in (Caruso et al., 2016) and according to the same protocol cellulose and hemicellulose parameters have been quantified also in IL 3-2 line. Briefly, a mixture of water, glacial acetic acid and sodium chlorite were added to dried samples and kept at 75 °C for 3 h. The residue was oven-dried at 105 °C for 24 h and treated with 100 mL of sodium hydroxide (4.4 mol L^{-1}) to calculate holocellulose. It was washed up with warm water (200 mL), 5 mL of acetic acid (2 mol L^{-1}) and 500 mL of water. Next, the residue was oven-dried at 105 °C for 24 h and weighed, providing the cellulose and pectin fraction. The hemi-cellulose content was calculated by subtracting the cellulose and pectin amount from that of holocellulose. Biomass dry powder (4 mg) was partially hydrolyzed by adding 0.5 mL of trifluoroacetic acid (2 mol L^{-1}). Vials were flushed with dry argon, mixed and heated at 100 °C for 4 h, cooled to room temperature and dried in evaporator. The pellets were washed with 500 μL of 2-propanol, vacuum dried and resuspended in 200 μL of deionised water, filtered with 0.45 μm PTFE filters, and analyzed by HPAEC. Monosaccharides were separated and quantified by HPAEC using a Dionex ICS-3000 with integrated amperometry detection. Chromatographic separation was performed on a CarboPac PA20 (3 × 150 mm) column (Thermo) using a gradient elution. The mobile phase consisted of: solution A, 100% water; solution B, 200 mM NaOH; solution C, 0.1 M sodium hydroxide, 0.5 M sodium acetate. A flow rate of 0.5 ml min^{-1} was used and the gradient was as follows: 0 min: 100% A; 5 min: 99% A, 1% B; 15 min: 99% A, 1% B; 22 min: 47.5% A, 22.5% B, 30% C; 30 min: 47.5% A, 22.5% B, 30% C. The column was then washed as follows: 30.1 min: 100% B; 37 min: 100% B; 37.1 min: 99% A, 1% B; 50 min: 100% A; 55 min: 100% A. The separated monosaccharides were quantified by using external calibration with a mixture of nine monosaccharide standards at 100 μM (arabinose, fucose, galactose, galacturonic acid, glucose, glucuronic acid, mannose, rhamnose, and xylose) that were subjected to acid hydrolysis in parallel with the samples. Data were processed to test the significance of component mean difference between IL2-6 and IL3-2 through a Student's t-test (P-value < 0.05).

2.8. Quantitative real-time PCR (qRT-PCR) analysis

Total RNA was extracted from leaves of plant samples as described previously. cDNA synthesis was performed with oligo (dT) and SuperScript III Reverse Transcriptase (Invitrogen). Specific primers pairs for the candidate genes (Supplementary Table S1) were designed using Primer3 software (http://primer3.ut.ee/). Quantitative real-time PCR (qRT–PCR) amplifications were performed on the 7900HT Fast Real-Time PCR System (Applied Biosystems, Foster City, CA, USA) using the SensiFAST SYBR Hi-ROX Kit (Bioline, Taunton, MA) with a 12.5 μL total volume mixture containing 4.5 μL of cDNA as the template. Three biological replicates and three technical replicates were carried out for each of the selected genes. The expression levels of the tested genes were normalized with an housekeeping gene coding for the elongation factor 1-α (Solyc06g005060), as an internal control, and relative gene expression was calculated with the $2^{-\triangle\triangle Ct}$ method (Livak and Schmittgen, 2001).

3. Results

3.1. Investigation of S. pennellii introgression lines transcriptome

The RNA sequencing of two nearly isogenic tomato *S. pennellii*, IL2-6 and IL3-2, generated a total of ~92 million of short reads sequences (Supplementary Table S2). In order to evaluate the effect of *S. pennellii* IGRs into the *S. lycopersicum* background, a gene expression profiling of the two contrasting lines for biomass traits, using SL2.5 as reference genome, was performed. IL2-6 and IL3-2 expressed 18832 and 17547 genes respectively, 1389 were exclusively expressed in IL2-6 and 604 in IL3-2 (Fig. 1A). More than 12926 differentially expressed genes (DEGs) with a FDR-adjusted P-value < 0.05, were identified between the two lines, including 7403 up-regulated genes and 5523 down-regulated genes (Fig. 1B). IL2-6 display 68 unique DEGS while IL3-2129 exclusively expressed DEGs (Supplementary Table S3).

The contribution of *S. pennellii* private genes to the two tomato nearly isogenic lines was evaluated by an IGR reads mapping on *S. pennelliii* (v2.0) genome coupled with a pairwise orthology analysis. Eight genes did not show orthologues to *S. lycopersicum* genome in IGR 2–6 and were considered unique of *S. pennellii* genome. Among these, Sopen02g034460, a proline-rich receptor-like protein kinase (PERK), involved in plant branching was expressed at high level compared with the others. As for as, an epimerase (Sopen02g034590) involved in metabolic processes and a cytochrome P450 (Sopen02g034950) involved in plant growth and development processes were also identified. A higher number of *S. pennelliii* private genes (70/877) were found in IGR 3–2. Among them, 68% (48/70) did not show known functions, suggesting that further studies are needed to understand their biological role, whereas the remaining genes do not seem to be involved in processes related to biomass production, except for a highly expressed

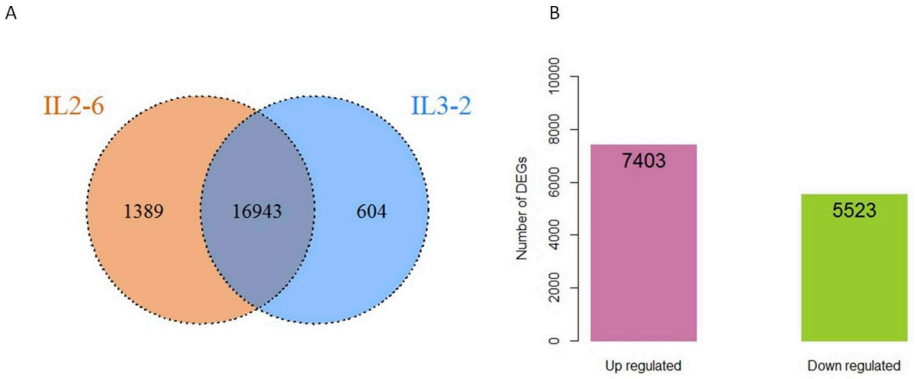

Fig. 1. Comparison of gene expression profile between IL2-6 and IL3-2. (A) Number of common and specific expressed genes in IL2-6 and IL3-2. (B) Number of differentially expressed genes (DEGs) identified in the comparison IL2-6 vs IL3-2 (FDR < 0.05).

ribulose bisphosphate carboxylase (RUBISCO) (Sopen03g007000).

3.2. Exploration of biological processes involved in biomass production

In order to gain more insights into DEGs function, a GO terms enrichment analysis was performed (Supplementary Tables S4 and S5 for a complete list of enriched GO terms). GO enriched categories for upregulated genes, related to biomass production, included development and photosynthesis processes as well as cell wall and carbohydrate metabolism (Fig. 2). Upregulated genes in IL2-6 were specifically enriched for processes associated to cell division as well as development and sucrose metabolism. The largest number of genes was included in the enriched GO terms: developmental process (375 genes), mitochondrion and chloroplast organization (66 and 68 genes), cell division (100 genes) and photosynthesis (99 genes, Supplementary Table S4). Five GO terms related to photosynthesis were enriched in IL2-6 and only one in IL3-2 (Fig. 2). IL3-2 also displayed overrepresented GO terms related to cell wall metabolism and biogenesis (cellulose metabolism, xylan metabolism etc) highlighting an extensive remodeling of its cell wall components (Fig. 2 and Supplementary Table S5).

3.3. Photosynthesis and related pathway

IL2-6 showed an activation of photosynthesis thanks to the higher number of upregulated genes in enriched GO terms related to this process. In particular, IL2-6 displayed an enrichment of upregulated genes involved in the light reaction and electron transport (Fig. 3A). Eight NADH dehydrogenase genes and many genes involved in the functioning of photosystem (PS) subunits PSI and PSII resulted upregulated, while 18 genes, components of the light harvesting complex II

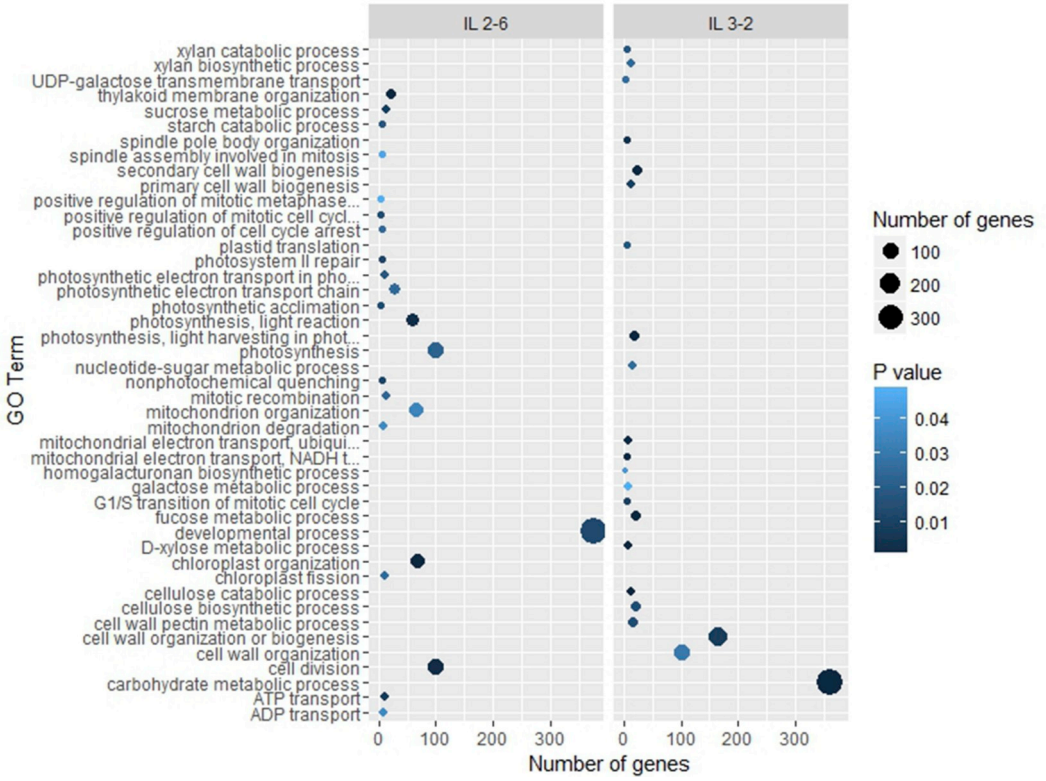

Fig. 2. Gene ontology (GO) enrichment analysis. Gene Ontology (GO) enrichment analysis at Biological Process (BP) level for differentially expressed genes (DEGs) between IL2-6 and IL3-2. IL2-6 = up regulated genes in IL2-6, IL3-2 = up regulated genes in IL3-2. The color gradient represents *P*-values and the differences in dot size correlate with the number of genes belonging to a particular GO term. Only GO terms showing a *P*-value < 0.05 are depicted. (For interpretation of the references to color in this figure legend, the reader is referred to the Web version of this article.)

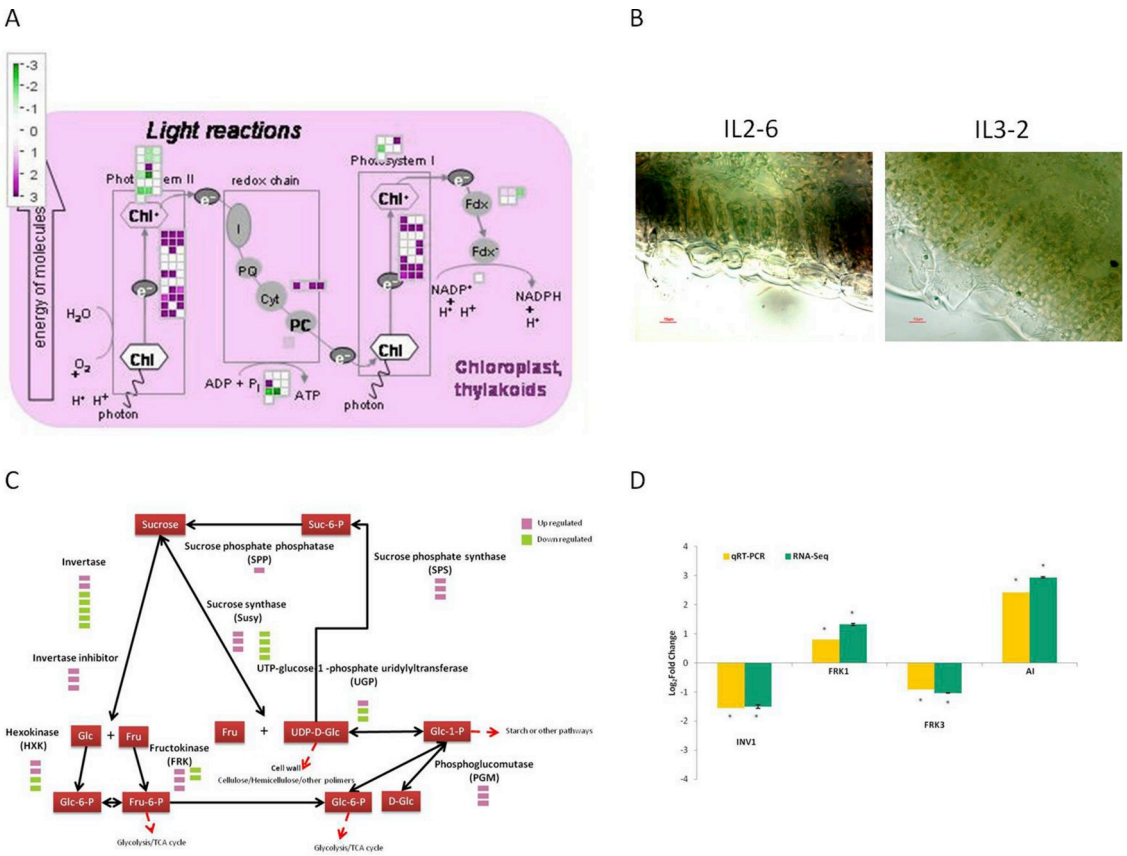

Fig. 3. Molecular characterization of photosynthesis and sucrose metabolism and morphology of leaf epidermal layer. (A) Differentially expressed genes (DEGs) in the Photosynthesis light reactions between IL2-6 and IL3-2. The colors purple and green indicate up and down regulated genes, respectively. (B) Microscopy analysis of the pattern of palisade cells in IL2-6 (left) and IL3-2 (right). (C) Schematic view of DEGs involved in carbon partitioning and allocation in IL-2-6 vs IL3-2. The colors purple and green indicate up and down regulated genes, respectively. (D) Gene expression on genes belonging to sucrose metabolism by qRT-PCR. The expression of invertase1 (INV1), Fructokinase 1 (FRK1), Fructokinase 3 (FRK3) and Acid invertase (AI) was measured by RNAseq (green bars) and qRT-PCR (yellow bars). The statistically significant differential gene expression was tested by the Student's t-test and likelihood ratio test (LRT) for qRT-PRC and RNA-Seq, respectively. The asterisks show the statistical significances (*: *P*-value < 0.05). Log_2 Fold Change: log_2 fold-change in gene expression between IL2-6 and IL3-2. (For interpretation of the references to color in this figure legend, the reader is referred to the Web version of this article.)

(LHCII), were downregulated. It is worth to note that IL2-6 exclusively expressed three genes of the photosystem II (Solyc01g007510, Solyc02g071030, Solyc01g102770) and a gene of photosystem I (Solyc05g056070) whilst IL3-2 exclusively expressed the ATP synthase (Solyc07g021380, Solyc12g006210, Supplemental Table S3). The per cell number of chloroplasts in the two tomato lines was almost similar, but they varied their size, with a chloroplast average area of 15.70 ± 3.42 μm^2 and 11.55 ± 2.27 μm^2 in IL2-6 and IL-32, respectively (Supplementary Table S6). Moreover, in IL2-6 the number of palisade chloroplasts for surface was almost double than in IL3-2 thanks to an higher number of cells for linear surface (12.57) compared to IL3-2 (7.29), at *P*-value < 0.01 (Fig. 3B, see also Supplementary Table S6).

In IL2-6 there was also an enrichment of genes associated to sucrose metabolic process (GO:0005985) including, among the others, three sucrose phosphate synthases (SPS, Solyc07g007790, Solyc08g042000, Solyc11g045110) and one sucrose phosphate phosphatase (SPP, Solyc10g081660, Fig. 3C). IL2-6 was also enriched in genes involved in ADP (GO:0015866) and ATP transport (GO:0015867) mainly inclusive of mitochondrial ADP/ATP carrier proteins as well as genes involved in starch metabolism (Fig. 2 and Supplementary Table S4). In the pathway of starch degradation four beta amylases were exclusively upregulated in IL2-6 and a higher number of alpha amylase (six) resulted activated in IL2-6 compared to IL3-2 (one). The gene expression of some key genes belonging to sucrose metabolism was also evaluated by qRT-PCR (Fig. 3D).

3.4. Cell cycle and developmental processes

IL2-6 showed the activation of auxin (indole-3-acetic acid, IAA) metabolism as suggested by the high number of upregulated genes involved in its synthesis (Supplementary Fig. S2) and signaling such as auxin regulated genes (12), including Auxin Response Factors family (ARFs) and Auxin Regulated gene involved in organ size (ARGOS, Solyc12g096570). Among the genes exclusively expressed in IL2-6 there were also six hormonal signal effectors belonging to SAUR and SAUR-like family proteins (Supplementary Table S3). On the other hand, IL3-2 showed a higher total number of upregulated genes associated to Aux/IAA family, suggesting that the auxin synthesis in the two lines starts from different substrates and follows separate routes modulated by specific regulators. Interesting DEGs related to gibberellin (i.e. Solyc03g006880), brassinosteroid metabolism (i.e. Solyc02g089160) and to meristem activity (i.e. Solyc12g020120, Solyc11g069470 and Solyc09g008250) were also found as well in the processes of the floral transition and flower formation (Supplementary Table S7).

The cell division resulted highly activated and cell cycle duration was shortened in IL2-6. An enrichment of the GO term “cell division” (including 100 genes) as well as in GO terms involved in the positive regulation of the cell cycle arrest and mitosis was observed in IL2-6. Fig. 4 describes the distribution of genes in enriched terms along the cell cycle phases. Among the genes exclusively expressed in IL2-6 there were a peptidyl-prolyl cis-trans isomerase (Solyc01g111170) related to cell cycle, and a regulator of chromosome condensation

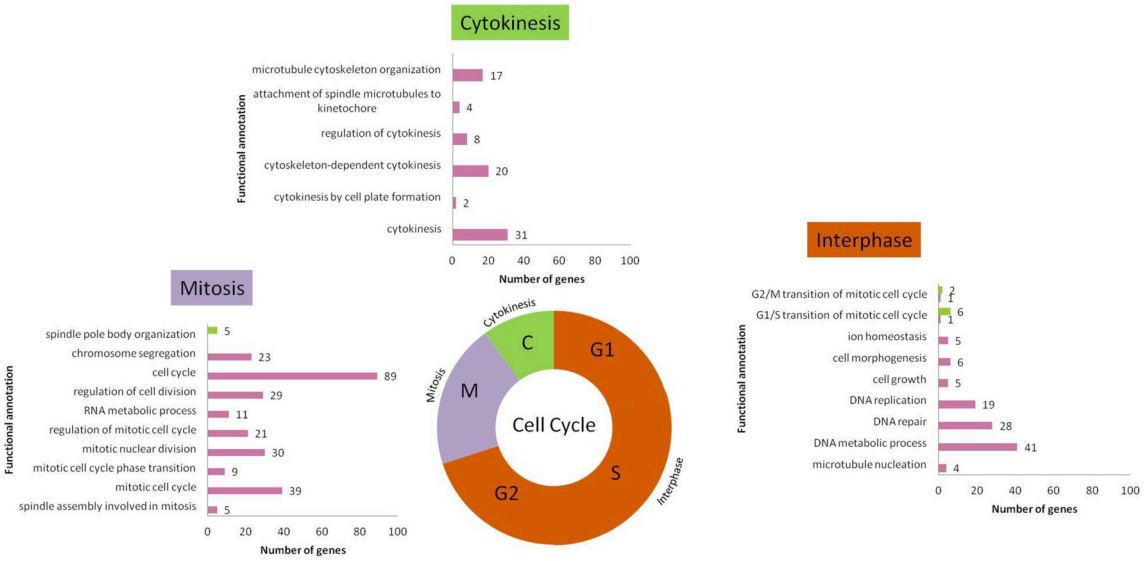

Fig. 4. Functional distribution of genes belonging to enriched Gene Ontology (GO) terms related to cell cycle along the cell cycle phases. The colors purple and green indicate up and down regulated genes, respectively. G1 = First gap, G2 = second gap and S = DNA synthesis. (For interpretation of the references to color in this figure legend, the reader is referred to the Web version of this article.)

(Solyc08g066570) related to cell division (Supplemental Table S3). IL2-6 exclusively upregulated four members of the E2F family and six APC genes, including the APC 10 (Solyc02g062680, Supplementary Table S7). By contrast, the GO terms "G1/S transition of mitotic cell cycle" and "spindle pole body organization" resulted enriched in IL3-2. In addition, three genes DA1 and one gene BIG BROTHER (BB) were simultaneously downregulated in IL3-2 (Supplemental Table S7). Interestingly, the number and the size of epidermal cells differed between the two lines. IL2-6 showed an higher number of cells for linear surface compared to IL3.2 (see above paragraph). The palisade cells in IL2-6 showed an average area of 277.50 ± 59.16 μm^2, while in the IL3-2 the average area corresponded to 493.45 ± 59.17 μm^2 (Supplementary Table S6). In addition, IL2-6 palisade cells had a typical cylindrical shape while IL3-2 cells had almost equal length and width (Fig. 3B).

3.5. Cell wall metabolism

Both primary and secondary cell wall synthesis and catabolism resulted triggered in IL3-2 with a high number of upregulated genes related to cellulose metabolism, including 20 genes involved in its biosynthesis (Cellulose synthase, COBRA-like protein, Alpha-1 4-glucan protein synthase) and 12 genes in its catabolism (Endoglucanase, Endo-beta-1 4-D-glucanase) producing in the end a moderate level of cellulose content (Supplementary Table S5 and Supplementary Fig. S3). By contrast, only the cellulose synthesis resulted activated in IL2-6 (Supplementary Fig. S3). In addition, the phenylpropanoid metabolism (lignin metabolism) resulted extremely challenged in IL2-6 (Fig. 5A). In particular, the phenylpropanoid synthesis showed an upregulation of genes located upstream to the formation of monolignols units (4-coumarate:CoA ligase, 4CL and p-hydroxycinnamoyltransferase, HCT) as well as in the last step (cinnamyl alcohol dehydrogenase, CAD). Moreover, many R2R3 TFs, known to be regulators of phenylpropanoid genes, resulted upregulated and an elevated lignin content was displayed in IL2-6 (Fig. 5B). Clear differences between the two lines were also observed in the hemicellulose and xylan metabolism, highlighting the general downregulation of hemicelluloses modifying enzymes such as Xyloglucan Endotransglycosylase/Hydrolase (XTH), xylosidase (XL), α-galactosidase (AGL), β-galactosidase (LAC), fucosidase (AFC), mannosidase (MND), xylanase (XLN) and related proteins such as expansins in IL2-6 (Fig. 5C). In the pathway of UDP-D-glucuronate biosynthesis (using as substrate the myo-inositol) four genes (Solyc02g093440, Solyc10g005400, Solyc12g008650, Solyc04g058070) were downregulated in IL2-6 leading to an increased content of D-glucuronate, a component of the hemicelluloses that was present at higher levels in IL2-6 (Fig. 5B and D). Indeed, important difference in hemicelluloses compounds abundance, such as fucose, galacturonic acid, glucose, glucuronic acid and mannose were pointed up (Fig. 5B).

4. Discussion

4.1. Differences in residual biomass production

Our study revealed that IL2-6 line has a more efficient biomass production thanks to a more effective coordination of chloroplasts and mitochondria energy fluxes to sustain growth. A higher rate of photosynthesis was observed and confirmed by the extensive activation of genes involved in photosynthesis light reactions and in the Calvin cycle and by a higher number of chloroplasts in palisade parenchyma cells detected per unit surface area. The elevated C supply obtained from chloroplasts provides abundant substrates for the subsequent C fixation and transformation.

4.2. Acceleration of photosynthesis process

A growing body of experimental evidences showed that increasing level of photosynthetic enzymes enhances photosynthesis and plant biomass production (Miyagawa et al., 2001; Lefebvre, 2005; Raines, 2006, 2011; Rosenthal et al., 2011; Uematsu et al., 2012; Simkin et al., 2015, 2017a; Driever et al., 2017). The boost of photosynthetic process in IL2-6 results in a higher supply of ATP and NADPH to reductive Calvin-Benson-Bassham (CBB) cycle to activate ribulose-1,5-bisphosphate carboxylase/oxygenase (RuBP) regeneration. In addition, the cytochrome *b*6/f complex in IL2-6, thanks to Rieske FeS protein (Solyc07g008310), promotes the CO_2 assimilation and plant growth (Yamori et al., 2016; Simkin et al., 2017b; Lima et al., 2017). Furthermore, Solyc04g051610, a Violaxanthin de-epoxidase-related protein (VDE), and Solyc02g090890, a zeaxanthin epoxidase (ZEP), in IL2-6 may accelerate the xanthophyll cycle IL2-6 and the non-photochemical quenching (NPQ) relaxation (decline) on the transfer of leaves from light to shade leading to a faster restoration of the maximum efficiency of CO_2 assimilation (Kromdijk et al., 2016). The sucrose on the other hand will be able to drive the cell proliferation and cell wall

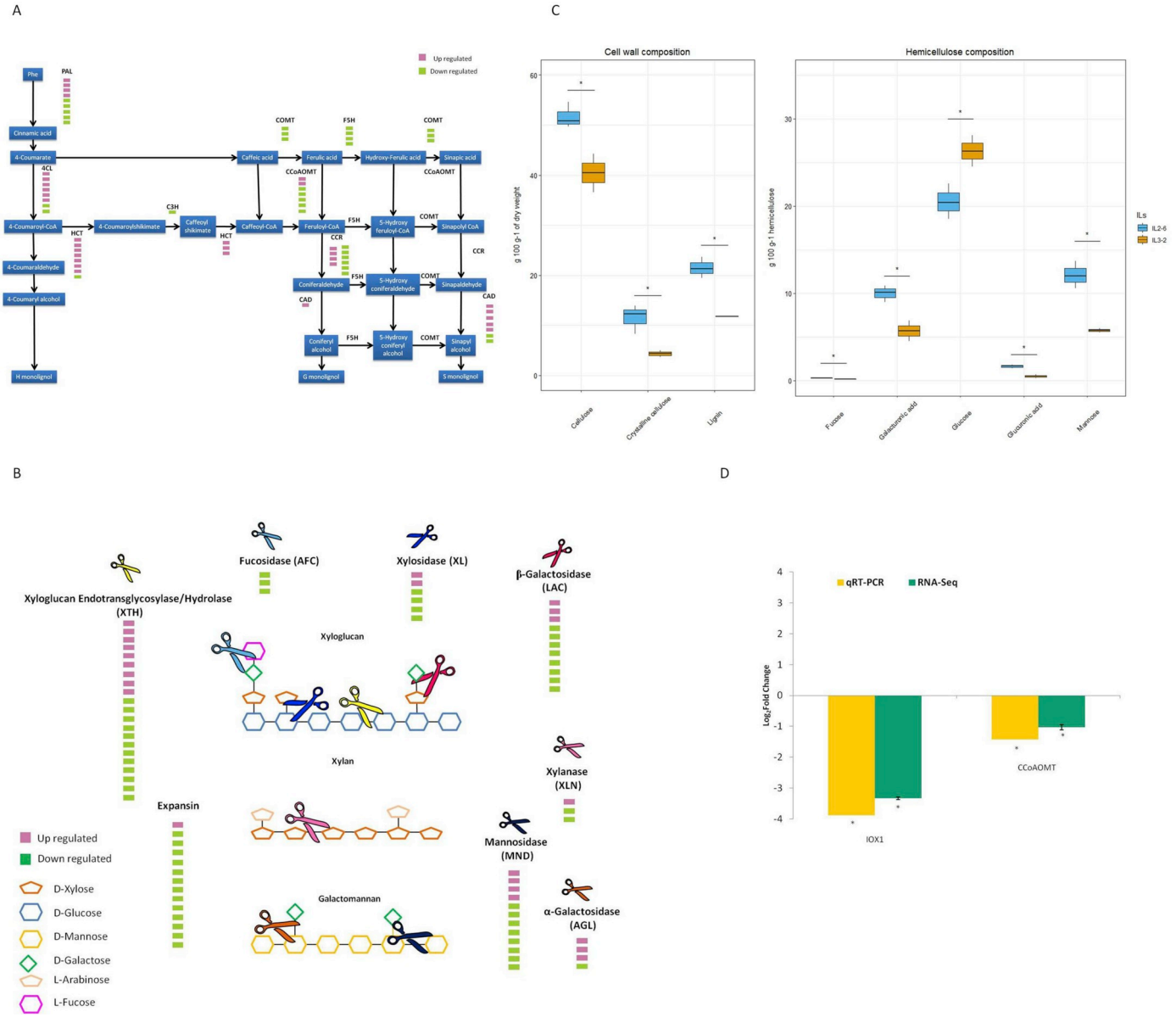

Fig. 5. Overview of cell wall dynamics at gene expression level (RNAseq and qRT-PCR) and chemical level. (A) Schematic view of differentially expressed genes (DEGs) involved in phenylpropanoid metabolism and lignin synthesis in IL2-6 vs IL3-2. The abbreviations: PAL, phenylalanine ammonia-lyase; C4H, cinnamate 4-hydroxylase; 4CL, 4-coumarate:CoA ligase; C3H, p-coumarate 3-hydroxylase; HCT, p-hydroxycinnamoyltransferase; CCoAOMT, caffeoyl-CoA O-methyltransferase; CCR, cinnamoyl-CoA reductase; F5H, ferulate 5-hydroxylase; COMT, caffeic acid O-methyltransferase; and CAD, cinnamyl alcohol dehydrogenase.(B) Difference in cell wall polymers and hemicelluloses monosaccharides content between IL2-6 and IL3-2. Statistical significance was determined using Student's *t*-test (*: *P*-value < 0.05). (C) Schematic view of DEGs involved in hemicellulose metabolism in IL2-6 vs IL3-2. (D) The expression of Inositol oxygenase (IOX1), Caffeoyl-CoA O-methyltransferase (CCoAOMT) was measured by RNAseq (green bars) and qRT-PCR (yellow bars). The statistically significant differential gene expression was tested by the Student's t-test and likelihood ratio test (LRT) for qRT-PRC and RNA-Seq, respectively. The asterisks show the statistical significances (*: *P*-value < 0.05). Log_2 Fold Change: log_2 fold-change in gene expression between IL2-6 and IL3-2. (For interpretation of the references to color in this figure legend, the reader is referred to the Web version of this article.)

synthesis promoting the building of different plant structures. The pathway of sucrose synthesis in IL2-6 is triggered through the upregulation of SPS and SPP that are known to increase plant growth and biomass accumulation in several plants (Maloney et al., 2015; Lima et al., 2017; Foyer and Ferrario, 1994; Laporte et al., 1997). The activation of mitochondrial genes transporting ATP, observed in IL2-6, not only supports the sucrose synthesis in the cytosol but also important functions, such as protein and cell wall synthesis. The high content of ATP and of energy molecule "sucrose" in turn may trigger the cell division and activate key genes involved in hormone and cell wall metabolism. The IL2-6 increased expression level of genes involved in starch degradation in light conditions suggests also a potential improvement of C use efficiency of this line. Remobilization of fixed C from starch reserves in the light would allow more of the available light energy (i.e. ATP and reducing power) to be used for biosynthesis of amino acids and other structural precursors required for growth (9). Indeed, a very robust negative correlation between starch content and biomass accumulation was revealed in *Arabidopsis* (Sulpice et al., 2009, 2010; Stitt and Zeeman, 2012).

4.3. Extension of vegetative phase and promotion of cell division activity

Prolonged vegetative meristem activity with concomitant increase in biomass yield was observed in several plants overexpressing

flowering-time genes (Demura and Ye, 2010; Salehi et al., 2005). Indeed, the activation of the flowering promoting factor-like1 (Solyc01g066980), early flowering 3 (Solyc06g062480, Solyc11g070100, Solyc12g095900) as well as of the flowering locus T1 (Solyc11g008650), C-like MADS-box protein (Solyc12g087810) and embryo flowering 1-like protein (Solyc11g071250) in IL2-6, supported the very late maturing performance and the excellent leaf coverage observed in field trials (Caruso et al., 2016). The IL2-6 line also showed the overexpression of ARGOS (Solyc12g096570) and Solyc03g006880, a gibberellin 20-oxidase-1 (Eriksson et al., 2000; Jeon et al., 2016; Voorend et al., 2016), suggesting that the growing period is extended by delaying the flowering time to give rise to larger plant and organ size (Hu et al., 2003). It is worth to note that in IL2-6 it was also observed the upregulation of Solyc12g009840, ortholog to AVP1 (Arabidopsis Vacuolar Pyrophosphatase 1, AT1G15690.1), a pyrophosphate-energized proton pump enzyme that maintains vacuolar turgor (Rojas et al., 2010), involved in the cell number increasing and subsequently in the size of leaves (Li et al., 2005; Lv et al., 2008; Gonzalez et al., 2010; S Khadilkar et al., 2016). Indeed, the field residual biomass and leaf expansion of IL 2–6 showed values ten times higher than IL 3–2 (Caruso et al., 2016).

The IL2-6 plant branching enhancement may be mediated by the overexpression of the DWARF gene Solyc02g089160, encoding a cytochrome P450, promoting a slender and compact plant architecture (Li et al., 2016). The activation of TFs belonging to GRF 1, 3 and 5 (Solyc04g077510, Solyc01g091540, Solyc08g075950, Solyc12g096070, Solyc08g005430) could result in the promotion of leaves growth (Kim et al., 2003; Rojas et al., 2010; Horiguchi et al., 2005), while the overexpression of REVOLUTA (Solyc12g020120 and Solyc11g069470) HD-zip III TFs and the MYB TF Blind gene (Solyc09g008250) may be involved in lateral meristems branching (Schmitz et al., 2002), supporting AMs organogenesis. In addition, a previous study pointed out that knock out (KO) of PERK gene family to which Sopen02g034460 belongs, promoted losses of apical dominance, increasing branching (Haffani et al., 2006).

The enlarged size and the higher number of palisade cells observed in IL2-6 could be related to the upregulation of the gene APC10 (Solyc02g062680) known to be a master regulator of cell division and increase of leaf size (Eloy et al., 2011; Lima et al., 2013) and of E2F genes, key cell cycle regulators, involved in plant growth promoting (Abraham and del Pozo, 2012). By contrast, in IL3-2 the enrichment in mitotic cell cycle regulation coupled with the upregulation of genes coding for the ubiquitin receptor DA1 (Solyc01g105180, Solyc04g079840, Solyc01g105210) and E3 ligase “BIG BROTHER” (BB, Solyc11g062260) can restrict the cell proliferation limiting the organ size (Disch et al., 2006; Li et al., 2008). The different epidermal cell morphology between the two lines can in turn also explain the variation in photosynthetic genes expression. In tomato ILs, leaf morphological traits showed to be correlated with expression of developmental and photosynthetic genes (Chitwood et al., 2013).

4.4. Effect of lignocellulosic biomass composition on saccharification rate

The different composition and organization of cell wall polysaccharides of IL lines affects biomass quality and hydrolysis of fermentable sugars. The activation of both cellulose synthesis and catabolism in IL3-2 resulted in limited amount of this polysaccharide, whilst the exclusive upregulation of genes involved in its synthesis found in IL2-6 increased the cellulose content and improved the saccharification rate (Caruso et al., 2016).

The lignin biosynthesis, and in particular the key conversion catalized by 4-coumarate:CoA ligase (4CL) of p-coumaric and caffeic acids to their thioester form during monolignol biosynthesis (Saballos et al., 2012), resulted greatly shifted in IL2-6. The upregulation of p-hydroxycinnamoyltransferase (HCT) observed in IL2-6 could explain the production of plants with higher lignin levels and altered lignin composition, thanks to the increase in syringyl aromatic (S) and Guaiacyl (G) units and a decrease in p-hydroxyphenyl (H) units (Shadle et al., 2007). The G and the S unit ratio determine the type and number of crosslinks, as well as the reactivity of the lignin (Kačík et al., 2012). The higher number of S units found in IL2-6 have a positive effect on the saccharification rate, since S units form C–C bonds and tend to form more linear chains and more β-β resin structures (Sorek et al., 2014; Cesarino et al., 2012).

By contrast, the elevated xylan content and the structure of hemicelluloses in IL3-2 resulted strongly modulated by the overexpression of transcripts involved in xylan acetylation and belonging to trichome birefringence-like (TBL) family such as Solyc12g014200, Solyc09g015350, Solyc09g007420 (Marriott et al., 2016) and Solyc02g093090, orthologous to Arabidopsis irregular xylem (irx) genes. The xylan abundance in IL3-2 could strengthen the cell wall making it less accessible to the enzymatic treatments in comparison to IL2-6. The content and composition of hemicellulose affects possible cross-links between hemicelluloses with cellulose and lignin, defining the cell-wall architecture and resistance to hydrolysis and degradability (Tavares et al., 2015). The acetyl groups block the access of hydrolytic enzymes to glycosidic linkages through steric hindrance (Biely et al., 1986). Irx mutants showed a reduced glucuronoxylan (GX) content in secondary cell walls and a significant increase in saccharification (Brown et al., 2007, 2011; Lee et al., 2007, 2009; Pena et al., 2007; Petersen et al., 2012). Moreover, the biomass quality and saccharification rate of IL3-2 may be negatively affected by side-chain substitution of xylan with glucuronic acid (GlcA) and the methylation of the GlcA residues in hemicellulose, mediated by the upregulation of glycogen like proteins Solyc11g005760 (GUX1), Solyc11g031950 (GXM3) and Solyc01g103360 (GXM1) (Lee et al., 2012; Urbanowicz et al., 2012). Finally, in IL3-2 the upregulation of GHMP kinase family protein (Solyc02g093440) and UDP-N-acetylglucosamine-pyrophosphorylase (Solyc04g058070) facilitated the conversion of glucuronic acid in UDP-glucuronic acid whilst the upregulation of two polygalacturonases, Solyc08g060970 and Solyc12g096730, converting respectively Digalacturonate in D-Galacturonate and Poly 1,4-α-D-galacturonate in D-galacturonate. Indeed, a clear enhanced glucuronate production was observed in IL2-6. By contrast, the activation of three Mannan endo-1 4-beta-mannosidases (Solyc04g080620, Solyc11g012190, Solyc12g013750) in IL2-6 promoted its high mannose hemicellulose content.

5. Conclusions

In summary, this study provides a modeling of processes underlying the biomass production and biomass quality for biofuel conversion in *Solanum lycopersicum*. The plant energy balance status of tomato plant resulted the major driver of biomass production. The transcriptomic analysis between high and low biomass lines showed that photosynthesis and cell division are pivotal processes to biomass accumulation. The molecular findings are supported by the different epidermal cell size and morphology observed in the two lines. The cell wall architecture is affected by fiber composition and specific polimer cross-linked organization. Our work improves knowledge on tomato biomass production and on its potential use for bioenergy purpose.

Data availability

Data deposition: Raw and processed sequence data, from IL2-6, IL3-2 and M82, supporting the findings of this study are available from the National Center for Biotechnology's (NCBI) Gene Expression Omnibus as GEO Series GSE128409.

Funding

This work was supported through the BIOMASSVAL project funded

by the Ministry of Agricultural, Food and Forestry Policies.

Acknowledgements

DD was centrally involved in transcriptomic analysis, interpretation of data and in manuscript writing; EC was involved in gene annotation, interpretation data and paper drafting; GA contributed to bioinformatics and statistical analysis, interpretation data and paper revision; FF was involved in phenotypic analysis and RNA extraction. CB contributed to gene expression analysis; GC was involved in chemical analysis and interpretation; ADN performed microscopy analysis and in morphological data interpretation; LF critically revised the manuscript; MRE conceived the study and was mainly involved in interpretation of data and in manuscript writing. All authors read and approved the final manuscript.

Appendix A. Supplementary data

Supplementary data to this article can be found online at https://doi.org/10.1016/j.plaphy.2019.08.010.

References

Abraham, Z., del Pozo, J.C., 2012. Ectopic expression of E2FB, a cell cycle transcription factor, accelerates flowering and increases fruit yield in tomato. J. Plant Growth Regul. 31, 11–24. https://doi.org/10.1007/s00344-011-9215-y.

Alexa, A., Rahnenfuhrer, J., 2018. Gene Set Enrichment Analysis with topGO. April 30. 2018.

Alexeyenko, A., Tamas, I., Liu, G., Sonnhammer, E.L.L., 2006. Automatic clustering of orthologs and inparalogs shared by multiple proteomes. Bioinformatics 22, 9–15. https://doi.org/10.1093/bioinformatics/btl213.

Anders, S., Pyl, P.T., Huber, W., 2015. HTSeq-A Python framework to work with high-throughput sequencing data. Bioinformatics 31, 166–169. https://doi.org/10.1093/bioinformatics/btu638.

Aro, E.M., 2016. From first generation biofuels to advanced solar biofuels. Ambio 45, 24–31. https://doi.org/10.1007/s13280-015-0730-0.

Baskar, C., Baskar, S., Dhillon, R.S., 2012. Biomass Conversion: the Interface of Biotechnology, Chemistry and Materials Science. https://doi.org/10.1007/978-3-642-28418-2.

Benjamini, Y., Hochberg, Y., 1995. Controlling the false discovery Rate : a practical and powerful approach to multiple testing author (s): yoav Benjamini and yosef Hochberg Source . J. R. Stat. Soc. B. 57, 289–300. https://doi.org/10.2307/2346101. Journal of the Royal Statistical Society . Series B (Methodological), Vol . 57 , No . 1 Published by.

Biely, P., Mackenzie, C.R., Puls, J., Schneider, H., 1986. Cooperativity of esterases and xylanases in the enzymatic degradation of acetyl xylan. Nat. Biotechnol. 4, 731–733.

Bolger, A.M., Lohse, M., Usadel, B., 2014a. Trimmomatic: a flexible trimmer for Illumina sequence data. Bioinformatics 30, 2114–2120. https://doi.org/10.1093/bioinformatics/btu170.

Bolger, A., Scossa, F., Bolger, M.E., et al., 2014b. The genome of the stress-tolerant wild tomato species Solanum pennellii. Nat. Genet. 46, 1034–1038.

Brown, D.M., Goubet, F., Wong, V.W., Goodacre, R., Stephens, E., Dupree, P., Turner, S.R., 2007. Comparison of five xylan synthesis mutants reveals new insight into the mechanisms of xylan synthesis. Plant J. 52, 1154–1168. https://doi.org/10.1111/j.1365-313X.2007.03307.x.

Brown, D., Wightman, R., Zhang, Z., Gomez, L.D., Atanassov, I., Bukowski, J.P., Tryfona, T., McQueen-Mason, S.J., Dupree, P., Turner, S., 2011. Arabidopsis genes IRREGULAR XYLEM (IRX15) and IRX15L encode DUF579-containing proteins that are essential for normal xylan deposition in the secondary cell wall. Plant J. 66, 401–413. https://doi.org/10.1111/j.1365-313X.2011.04501.x.

Caruso, G., Gomez, L.D., Ferriello, F., Andolfi, A., Borgonuovo, C., Evidente, A., Simister, R., McQueen-Mason, S.J., Carputo, D., Frusciante, L., Ercolano, M.R., 2016. Exploring tomato Solanum pennellii introgression lines for residual biomass and enzymatic digestibility traits. BMC Genet. 17, 1–13. https://doi.org/10.1186/s12863-016-0362-9.

Cesarino, I., Araújo, P., Sampaio Mayer, J.L., Paes Leme, A.F., Mazzafera, P., 2012. Enzymatic activity and proteomic profile of class III peroxidases during sugarcane stem development. Plant Physiol. Biochem. 55, 66–76.

Chitwood, D.H., Kumar, R., Headland, L.R., Ranjan, A., Covington, M.F., Ichihashi, Y., Fulop, D., Jiménez-Gómez, J.M., Peng, J., Maloof, J.N., Sinha, N.R., 2013. A quantitative genetic basis for leaf morphology in a set of precisely defined tomato introgression lines. Plant Cell 25, 2465–2481.

De Veylder, L., Beeckman, T., Inzé, D., 2007. The ins and outs of the plant cell cycle. Nat. Rev. Mol. Cell Biol. 8, 655–665. https://doi.org/10.1038/nrm2227.

Demura, T., Ye, Z.H., 2010. Regulation of plant biomass production. Curr. Opin. Plant Biol. 13, 299–304. https://doi.org/10.1016/j.pbi.2010.03.002.

Disch, S., Anastasiou, E., Sharma, V.K., Laux, T., Fletcher, J.C., Lenhard, M., 2006. The E3 ubiquitin ligase BIG BROTHER controls Arabidopsis organ size in a dosage-dependent manner. Curr. Biol. 16, 272–279. https://doi.org/10.1016/j.cub.2005.12.026.

Driever, S.M., Simkin, A.J., Alotaibi, S., Fisk, S.J., Madgwick, P.J., Sparks, C.A., Jones, H.D., Lawson, T., Parry, M.A.J., Raines, C.A., 2017. Increased sbpase activity improves photosynthesis and grain yield in wheat grown in greenhouse conditions. Philos. Trans. R. Soc. Biol. Sci. 372. https://doi.org/10.1098/rstb.2016.0384.

Eloy, N.B., De Freitas Lima, M., Van Damme, D., Vanhaeren, H., Gonzalez, N., De Milde, L., Hemerly, A.S., Beemster, G.T.S., Inzé, D., Ferreira, P.C.G., 2011. The APC/C subunit 10 plays an essential role in cell proliferation during leaf development. Plant J. 68, 351–363. https://doi.org/10.1111/j.1365-313X.2011.04691.x.

Eloy, N.B., de Freitas Lima, M., Ferreira, P.C.G., Inzé, D., 2015. The role of the anaphase-promoting complex/cyclosome in plant growth. CRC Crit. Rev. Plant Sci. 34, 487–505. https://doi.org/10.1080/07352689.2015.1078613.

Ercolano, M.R., Gomez, L.D., Andolfi, A., Simister, R., Troise, C., Angelino, G., Borrelli, C., McQueen-Mason, S.J., Evidente, A., Frusciante, L., Caruso, G., 2015. Residual biomass saccharification in processing tomato is affected by cultivar and nitrogen fertilization. Biomass Bioenergy 72, 242–250. https://doi.org/10.1016/j.biombioe.2014.10.030.

Eriksson, M.E., Israelsson, M., Olsson, O., Moritz, T., 2000. Increased gibberellin biosynthesis in transgenic trees promotes growth, biomass production and xylem fiber length. Nat. Biotechnol. 18, 784–788.

Eshed, Y., Zamir, D., 1995. An introgression line population of Lycopersicon pennellii in the cultivated tomato enables the identification and fine mapping of yield- associated QTL. Genetics 141, 1147–1162. https://doi.org/10.1016/j.jhazmat.2011.11.031.

Fernandez, O., Ishihara, H., George, G.M., Mengin, V., Flis, A., Sumner, D., Arrivault, S., Feil, R., Lunn, J.E., Zeeman, S.C., Smith, A.M., Stitt, M., 2017. Leaf starch turnover occurs in long days and in falling light at the end of the day. Plant Physiol. 174, 2199–2212. https://doi.org/10.1104/pp.17.00601.

Foyer, C.H., Ferrario, S., 1994. Modulation of carbon and nitrogen-metabolism in transgenic plants with a view to improved biomass production. Biochem. Soc. Trans. 22, 909–915.

Gomez, L.D., Amalfitano, C., Andolfi, A., Simister, R., Somma, S., Ercolano, M.R., Borrelli, C., McQueen-Mason, S.J., Frusciante, L., Cuciniello, A., Caruso, G., 2017. Valorising faba bean residual biomass: effect of farming system and planting time on the potential for biofuel production. Biomass Bioenergy 107, 227–232.

Gonzalez, N., De Bodt, S., Sulpice, R., Jikumaru, Y., Chae, E., Dhondt, S., Van Daele, T., De Milde, L., Weigel, D., Kamiya, Y., Stitt, M., Beemster, G.T.S., Inze, D., 2010. Increased leaf size: different means to an end. Plant Physiol. 153, 1261–1279. https://doi.org/10.1104/pp.110.156018.

Haffani, Y.Z., Silva-Gagliardi, N.F., Sewter, S.K., Aldea, M.G., Zhao, Z., Nakhamchik, A., Cameron, R.K., Goring, D.R., 2006. Altered expression of PERK receptor kinases in arabidopsis leads to changes in growth and floral organ formation. Plant Signal. Behav. 1, 251–260. https://doi.org/10.4161/psb.1.5.3324.

Horiguchi, G., Kim, G.T., Tsukaya, H., 2005. The transcription factor AtGRF5 and the transcription coactivator AN3 regulate cell proliferation in leaf primordia of Arabidopsis thaliana. Plant J. 43, 68–78. https://doi.org/10.1111/j.1365-313X.2005.02429.x.

Hu, Y., Xie, Q., Chua, N.H., 2003. The Arabidopsis auxin-inducible gene ARGOS controls lateral organsize. Plant Cell 15, 1951–1961.

Inzé, D., 2003. Why should we study the plant cell cycle? J. Exp. Bot. 54, 1125–1126. https://doi.org/10.1093/jxb/erg138.

Isikgor, F.H., Becer, C.R., 2015. Lignocellulosic biomass: a sustainable platform for the production of bio-based chemicals and polymers. Polym. Chem. 6, 4497–4559. https://doi.org/10.1039/c5py00263j.

Jeon, H.W., Cho, J.S., Park, E.J., Han, K.H., Choi, Y.I., Ko, J.H., 2016. Developing xylem-preferential expression of PdGA20ox1, a gibberellin 20-oxidase 1 from Pinus densiflora, improves woody biomass production in a hybrid poplar. Plant Biotechnol. J. 14, 1161–1170. https://doi.org/10.1111/pbi.12484.

Joung, J.-G., Corbett, A.M., Fellman, S.M., Tieman, D.M., Klee, H.J., Giovannoni, J.J., Fei, Z., 2009. Plant MetGenMAP: an integrative analysis system for plant systems biology. Plant Physiol. 151, 1758–1768. https://doi.org/10.1104/pp.109.145169.

Kačík, F., Ďurkovič, J., Kačíková, D., 2012. Chemical profiles of wood components of poplar clones for their energy utilization. Energies 5, 5243–5256. https://doi.org/10.3390/en5125243.

Kim, J.H., Choi, D., Kende, H., 2003. The AtGRF family of putative transcription factors is involved in leaf and cotyledon growth in Arabidopsis. Plant J. 36, 94–104. https://doi.org/10.1046/j.1365-313X.2003.01862.x.

Kim, D., Pertea, G., Trapnell, C., Pimentel, H., Kelley, R., Salzberg, S.L., 2013. TopHat2: accurate alignment of transcriptomes in the presence of insertions, deletions and gene fusions. Genome Biol. 14, R36. https://doi.org/10.1186/gb-2013-14-4-r36.

Koçar, G., Civaş, N., 2013. An overview of biofuels from energy crops: current status and future prospects. Renew. Sustain. Energy Rev. 28, 900–916. https://doi.org/10.1016/j.rser.2013.08.022.

Kromdijk, J., Głowacka, K., Leonelli, L., Gabilly, S.T., Iwai, M., Niyogi, K.K., Long, S.P., 2016. Improving photosynthesis and crop productivity by accelerating recovery from photoprotection. Science 354, 857–861. https://doi.org/10.1126/science.aai8878. 80-.

Laporte, M.M., Galagan, J.A., Shapiro, J.A., Boersig, M.R., Shewmaker, C.K., Sharkey, T.D., 1997. Sucrose-phosphate synthase activity and yield analysis of tomato plants transformed with maize sucrose-phosphate synthase. Planta 203, 253–259.

Lee, C., O'Neill, M.A., Tsumuraya, Y., Darvill, A.G., Ye, Z.H., 2007. The irregular xylem9 mutant is deficient in Xylan xylosyltransferase activity. Plant Cell Physiol. 48, 1624–1634. https://doi.org/10.1093/pcp/pcm135.

Lee, C., Teng, Q., Huang, W., Zhong, R., Ye, Z.H., 2009. Down-regulation of PoGT47C expression in poplar results in a reduced glucuronoxylan content and an increased wood digestibility by cellulase. Plant Cell Physiol. 50, 1075–1089. https://doi.org/10.1093/pcp/pcp060.

Lee, C., Teng, Q., Zhong, R., Ye, Z.H., 2012. Arabidopsis GUX proteins are

glucuronyltransferases responsible for the addition of glucuronic acid side chains onto xylan. Plant Cell Physiol. 53, 1204–1216. https://doi.org/10.1093/pcp/pcs064.
Lefebvre, S., 2005. Increased sedoheptulose-1,7-bisphosphatase activity in transgenic tobacco plants stimulates photosynthesis and growth from an early stage in development. Plant Physiol. 138, 451–460. https://doi.org/10.1104/pp.104.055046.
Li, J., Yang, H., Peer, W.A., Richter, G., Blakeslee, J., Bandyopadhyay, A., Titapiwantakun, B., Undurraga, S., Khodakovskaya, M., Richards, E.L., Krizek, B., Murphy, A.S., Gilroy, S., Gaxiola, R., 2005. Plant Science: arabidopsis H + -PPase AVP1 regulates auxin-mediated organ development. Science 310, 121–125 80-.
Li, Y., Zheng, L., Corke, F., Smith, C., Bevan, M.W., 2008. Control of final seed and organ size by the DA1 gene family in Arabidopsis thaliana. Genes Dev. 22, 1331–1336. https://doi.org/10.1101/gad.463608.
Li, H., Handsaker, B., Wysoker, A., Fennell, T., Ruan, J., Homer, N., Marth, G., Abecasis, G., Durbin, R., 2009. The sequence alignment/map format and SAMtools. Bioinformatics 25, 2078–2079. https://doi.org/10.1093/bioinformatics/btp352.
Li, X.J., Chen, X.J., Guo, X., Yin, L.L., Ahammed, G.J., Xu, C.J., Chen, K.S., Liu, C.C., Xia, X.J., Shi, K., Zhou, J., Zhou, Y.H., Yu, J.Q., 2016. DWARF overexpression induces alteration in phytohormone homeostasis, development, architecture and carotenoid accumulation in tomato. Plant Biotechnol. J. 14, 1021–1033. https://doi.org/10.1111/pbi.12474.
Lima, M. de F., Eloy, N.B., Pegoraro, C., Sagit, R., Rojas, C., Bretz, T., Vargas, L., Elofsson, A., de Oliveira, A.C., Hemerly, A.S., Ferreira, P.C., 2010. Genomic evolution and complexity of the Anaphase-promoting Complex (APC) in land plants. BMC Plant Biol. 10, 254. https://doi.org/10.1186/1471-2229-10-254.
Lima, M.D., Eloy, N.B., Bottino, M.C., Hemerly, A.S., Ferreira, P.C.G., 2013. Overexpression of the anaphase-promoting complex (APC) genes in Nicotiana tabacum promotes increasing biomass accumulation. Mol. Biol. Rep. 40, 7093–7102.
Lima, M. de F., Eloy, N.B., de Siqueira, J.A.B., Inzé, D., Hemerly, A.S., Ferreira, P.C.G., 2017. Molecular mechanisms of biomass increase in plants. Biotechnol. Res. Innov. https://doi.org/10.1016/j.biori.2017.08.001.
Livak, K.J., Schmittgen, T.D., 2001. Analysis of relative gene expression data using real-time quantitative PCR and the 2-ΔΔCT method. Methods 25, 402–408. https://doi.org/10.1006/meth.2001.1262.
Lv, S., Zhang, K., Gao, Q., Lian, L., Song, Y., Zhang, J., 2008. Overexpression of an H + -PPase gene from Thellungiella halophila in cotton enhances salt tolerance and improves growth and photosynthetic performance. Plant Cell Physiol. 49, 1150–1164. https://doi.org/10.1093/pcp/pcn090.
Maloney, V.J., Park, J.Y., Unda, F., Mansfield, S.D., 2015. Sucrose phosphate synthase and sucrose phosphate phosphatase interact in planta and promote plant growth and biomass accumulation. J. Exp. Bot. 66, 4383–4394. https://doi.org/10.1093/jxb/erv101.
Marriott, P.E., Gómez, L.D., Mcqueen-Mason, S.J., 2016. Unlocking the potential of lignocellulosic biomass through plant science. New Phytol. 209, 1366–1381. https://doi.org/10.1111/nph.13684.
Mckendry, P., 2002. Energy production from biomass (part 1): overview of biomass. Bioresour. Technol. 83, 37–46. https://doi.org/10.1016/s0960-8524(01)00118-3.
Miyagawa, Y., Tamoi, M., Shigeoka, S., 2001. Over-expression of a cyanobacterial fructose-1,6-sedoheptulose-1,7-bisphosphatase in tobacco enhances photosynthesis and growth. Nat. Biotechnol. 19, 965–969.
Omidbakhshfard, M.A., Proost, S., Fujikura, U., Mueller-Roeber, B., 2015. Growth-regulating factors (GRFs): a small transcription factor family with important functions in plant biology. Mol. Plant 8, 998–1010. https://doi.org/10.1016/j.molp.2015.01.013.
Pajoro, A., Madrigal, P., Muiño, J.M., Matus, J.T., Jin, J., Mecchia, M.A., Debernardi, J.M., Palatnik, J.F., Balazadeh, S., Arif, M., Ó'Maoiléidigh, D.S., Wellmer, F., Krajewski, P., Riechmann, J.L., Angenent, G.C., Kaufmann, K., 2014. Dynamics of chromatin accessibility and gene regulation by MADS-domain transcription factors in flower development. Genome Biol. 15. https://doi.org/10.1186/gb-2014-15-3-r41.
Peel, M.C., Finlayson, B.L., McMahon, T.A., 2007. Updated world map of the Koppen-Geiger climate classification. Hydrol. Earth Syst. Sci. 11, 1633e44.
Pena, M.J., Zhong, R., Zhou, G.-K., Richardson, E.A., O'Neill, M.A., Darvill, A.G., York, W.S., Ye, Z.-H., 2007. Arabidopsis irregular xylem8 and irregular xylem9: implications for the complexity of glucuronoxylan biosynthesis. Plant Cell Online 19, 549–563. https://doi.org/10.1105/tpc.106.049320.
Peña-Castro, J.M., Del Moral, S., Núñez-López, L., Barrera-Figueroa, B.E., Amaya-Delgado, L., 2017. Biotechnological strategies to improve plant biomass quality for bioethanol production. BioMed Res. Int. 2017. https://doi.org/10.1155/2017/7824076.
Petersen, P.D., Lau, J., Ebert, B., Yang, F., Verhertbruggen, Y., Kim, J.S., Varanasi, P., Suttangkakul, A., Auer, M., Loque, D., Scheller, H.V., 2012. Engineering of plants with improved properties as biofuels feedstocks by vessel-specific complementation of xylan biosynthesis mutants. Biotechnol. Biofuels 5, 84.
Raines, C.A., 2006. Transgenic approaches to manipulate the environmental responses of the C3 carbon fixation cycle. Plant Cell Environ. 29, 331–339. https://doi.org/10.1111/j.1365-3040.2005.01488.x.
Raines, C.A., 2011. Increasing photosynthetic carbon assimilation in C3 plants to improve crop yield: current and future strategies. Plant Physiol. 155, 36–42. https://doi.org/10.1104/pp.110.168559.
Remm, M., Storm, C.E., Sonnhammer, E.L., 2001. Automatic clustering of orthologs and in-paralogs from pairwise species comparisons. J. Mol. Biol. 314, 1041–1052.
Robinson, M.D., McCarthy, D.J., Smyth, G.K., edgeR, 2009. A Bioconductor package for differential expression analysis of digital gene expression data. Bioinformatics 26, 139–140. https://doi.org/10.1093/bioinformatics/btp616.
Rojas, C.A., Hemerly, A.S., Ferreira, P.C.G., 2010. Genetically modified crops for biomass increase. Genes and strategies. GM Crops 1, 137–142. https://doi.org/10.4161/gmcr.1.3.12615.
Rosenthal, D.M., Locke, A.M., Khozaei, M., Raines, C.A., Long, S.P., Ort, D.R., 2011. Over-expressing the C3photosynthesis cycle enzyme Sedoheptulose-1-7 Bisphosphatase improves photosynthetic carbon gain and yield under fully open air CO2fumigation (FACE). BMC Plant Biol. 11. https://doi.org/10.1186/1471-2229-11-123.
Ross, J.J., Quittenden, L.J., 2016. Interactions between brassinosteroids and gibberellins: synthesis or signaling? Plant Cell 28https://doi.org/10.1105/tpc.15.00917. tpc.00917.2015.
Ruan, Y.P., 2014. Sucrose Metabolism: gateway to diverse carbon use and sugar signaling. Annu. Rev. Plant Biol. 65, 33–67.
S Khadilkar, A., Yadav, U.P., Salazar, C., Shulaev, V., Paez-Valencia, J., Pizzio, G.A., Gaxiola, R.A., Ayre, B.G., 2016. Constitutive and companion cell-specific over-expression of *AVP1* , encoding a proton-pumping Pyrophosphatase, enhances biomass accumulation, phloem loading, and long-distance transport. Plant Physiol. 170, 401–414.
Saballos, A., Sattler, S.E., Sanchez, E., Foster, T.P., Xin, Z., Kang, C., Pedersen, J.F., Vermerris, W., 2012. Brown midrib2 (Bmr2) encodes the major 4-coumarate: coenzyme A ligase involved in lignin biosynthesis in sorghum (Sorghum bicolor (L.) Moench). Plant J. 70, 818–830. https://doi.org/10.1111/j.1365-313X.2012.04933.x.
Sablowski, R., Carnier Dornelas, M., 2014. Interplay between cell growth and cell cycle in plants. J. Exp. Bot. 65, 2703–2714. https://doi.org/10.1093/jxb/ert354.
Salehi, H., Ransom, C.B., Oraby, H.F., Seddighi, Z., Sticklen, M.B., 2005. Delay in flowering and increase in biomass of transgenic tobacco expressing the Arabidopsis floral repressor gene FLOWERING LOCUS C. J. Plant Physiol. 162, 711–717. https://doi.org/10.1016/j.jplph.2004.12.002.
Schmitz, G., Tillmann, E., Carriero, F., Fiore, C., Cellini, F., Theres, K., 2002. The tomato Blind gene encodes a MYB transcription factor that controls the formation of lateral meristems. Proc. Natl. Acad. Sci. 99, 1064–1069. https://doi.org/10.1073/pnas.022516199.
Shadle, G., Chen, F., Srinivasa Reddy, M.S., Jackson, L., Nakashima, J., Dixon, R.A., 2007. Down-regulation of hydroxycinnamoyl CoA: shikimate hydroxycinnamoyl transferase in transgenic alfalfa affects lignification, development and forage quality. Phytochemistry 68, 1521–1529.
Simkin, A.J., McAusland, L., Headland, L.R., Lawson, T., Raines, C.A., 2015. Multigene manipulation of photosynthetic carbon assimilation increases CO_2 fixation and biomass yield in tobacco. J. Exp. Bot. 66, 4075–4090. https://doi.org/10.1093/jxb/erv204.
Simkin, A.J., Lopez-Calcagno, P.E., Davey, P.A., Headland, L.R., Lawson, T., Timm, S., Bauwe, H., Raines, C.A., 2017a. Simultaneous stimulation of sedoheptulose 1,7-bisphosphatase, fructose 1,6-bisphophate aldolase and the photorespiratory glycine decarboxylase-H protein increases CO2assimilation, vegetative biomass and seed yield in Arabidopsis. Plant Biotechnol. J. 15, 805–816. https://doi.org/10.1111/pbi.12676.
Simkin, A.J., McAusland, L., Lawson, T., Raines, C.A., 2017b. Over-expression of the RieskeFeS protein increases electron transport rates and biomass yield. Plant Physiol., 00622. https://doi.org/10.1104/pp.17.00622. 2017.
Slavov, G., Allison, G., Bosch, M., 2013. Advances in the genetic dissection of plant cell walls: tools and resources available in Miscanthus. Front. Plant Sci. 4, 1–21. https://doi.org/10.3389/fpls.2013.00217.
Somerville, C., Youngs, H., Taylor, C., Davis, S.C., Long, S.P., 2010. Feedstocks for lignocellulosic biofuels. Science 329, 790–792. https://doi.org/10.1126/science.1189268. 80.
Sorek, N., Yeats, T.H., Szemenyei, H., Youngs, H., Somerville, C.R., 2014. The implications of lignocellulosic biomass chemical composition for the production of advanced biofuels. Bioscience 64, 192–201. https://doi.org/10.1093/biosci/bit037.
Stitt, M., Zeeman, S.C., 2012. Starch turnover: pathways, regulation and role in growth. Curr. Opin. Plant Biol. 15, 282–292. https://doi.org/10.1016/j.pbi.2012.03.016.
Sulpice, R., Pyl, E.-T., Ishihara, H., Trenkamp, S., Steinfath, M., Witucka-Wall, H., Gibon, Y., Usadel, B., Poree, F., Piques, M.C., Von Korff, M., Steinhauser, M.C., Keurentjes, J.J.B., Guenther, M., Hoehne, M., Selbig, J., Fernie, A.R., Altmann, T., Stitt, M., 2009. Starch as a major integrator in the regulation of plant growth. Proc. Natl. Acad. Sci. 106, 10348–10353. https://doi.org/10.1073/pnas.0903478106.
Sulpice, R., Trenkamp, S., Steinfath, M., Usadel, B., Gibon, Y., Witucka-Wall, H., Pyl, E.-T., Tschoep, H., Steinhauser, M.C., Guenther, M., Hoehne, M., Rohwer, J.M., Altmann, T., Fernie, A.R., Stitt, M., 2010. Network analysis of enzyme activities and metabolite levels and their relationship to biomass in a large panel of arabidopsis accessions. Plant Cell 22, 2872–2893. https://doi.org/10.1105/tpc.110.076653.
Tavares, E.Q.P., De Souza, A.P., Buckeridge, M.S., 2015. How endogenous plant cell-wall degradation mechanisms can help achieve higher efficiency in saccharification of biomass. J. Exp. Bot. 66, 4133–4143. https://doi.org/10.1093/jxb/erv171.
Thimm, O., Bläsing, O., Gibon, Y., Nagel, A., Meyer, S., Krüger, P., Selbig, J., Müller, L.A., Rhee, S.Y., Stitt, M., 2004. MAPMAN: a user-driven tool to display genomics data sets onto diagrams of metabolic pathways and other biological processes. Plant J. 37, 914–939. https://doi.org/10.1111/j.1365-313X.2004.02016.x.
Tognetti, J.A., Pontis, H.G., Martínez-Noël, G.M.A., 2013. Sucrose signaling in plants: a world yet to be explored, Plant Signal. Beyond Behav. 8. https://doi.org/10.4161/psb.23316.
Uematsu, K., Suzuki, N., Iwamae, T., Inui, M., Yukawa, H., 2012. Increased fructose 1,6-bisphosphate aldolase in plastids enhances growth and photosynthesis of tobacco plants. J. Exp. Bot. 63, 3001–3009. https://doi.org/10.1093/jxb/ers004.
Urbanowicz, B.R., Pena, M.J., Ratnaparkhe, S., Avci, U., Backe, J., Steet, H.F., Foston, M., Li, H., O'Neill, M.A., Ragauskas, A.J., Darvill, A.G., Wyman, C., Gilbert, H.J., York, W.S., 2012. 4-O-methylation of glucuronic acid in Arabidopsis glucuronoxylan is catalyzed by a domain of unknown function family 579 protein. Proc. Natl. Acad. Sci. 109, 14253–14258. https://doi.org/10.1073/pnas.1208097109.
Van Bel, M., Diels, T., Vancaester, E., Kreft, L., Botzki, A., Van De Peer, Y., Coppens, F., Vandepoele, K., 2018. PLAZA 4.0: an integrative resource for functional, evolutionary and comparative plant genomics. Nucleic Acids Res. 46, D1190–D1196. https://doi.

org/10.1093/nar/gkx1002.
Vanholme, B., Desmet, T., Ronsse, F., Rabaey, K., Van Breusegem, F., De Mey, M., Soetaert, W., Boerjan, W., 2013. Towards a carbon-negative sustainable bio-based economy. Front. Plant Sci. 4. https://doi.org/10.3389/fpls.2013.00174.
Voorend, W., Nelissen, H., Vanholme, R., De Vliegher, A., Van Breusegem, F., Boerjan, W., Roldán-Ruiz, I., Muylle, H., Inzé, D., 2016. Overexpression of GA20-OXIDASE1 impacts plant height, biomass allocation and saccharification efficiency in maize. Plant Biotechnol. J. 14, 997–1007. https://doi.org/10.1111/pbi.12458.
Wade Harper, J., Burton, J.L., Solomon, M.J., 2002. The anaphase-promoting complex: it's not just for mitosis any more. Genes Dev. 16, 2179–2206. https://doi.org/10.1101/gad.1013102.
Yamori, W., Kondo, E., Sugiura, D., Terashima, I., Suzuki, Y., Makino, A., 2016. Enhanced leaf photosynthesis as a target to increase grain yield: insights from transgenic rice lines with variable Rieske FeS protein content in the cytochrome b6/f complex. Plant Cell Environ. 39, 80–87. https://doi.org/10.1111/pce.12594.
Yang, M., Jiao, Y., 2016. Regulation of axillary meristem initiation by transcription factors and plant hormones. Front. Plant Sci. 7, 1–6. https://doi.org/10.3389/fpls.2016.00183.
Zhou, C.H., Xia, X., Lin, C.X., Tong, D.S., Beltramini, J., 2011. Catalytic conversion of lignocellulosic biomass to fine chemicals and fuels. Chem. Soc. Rev. 40, 5588–5617. https://doi.org/10.1039/c1cs15124j.